Signal to noise and signal to noise efficiency in SMASH imaging

ARTICLE *in* MAGNETIC RESONANCE IN MEDICINE · JUNE 1999

Impact Factor: 3.57 · DOI: 10.1002/(SICI)1522-2594(199905)41:5<1009::AID-MRM21>3.0.CO;2-4 · Source: PubMed

5 AUTHORS, INCLUDING:

Daniel Sodickson
New York University
212 PUBLICATIONS **5,817** CITATIONS
SEE PROFILE

Mark Griswold
Case Western Reserve University
197 PUBLICATIONS **5,930** CITATIONS
SEE PROFILE

Peter M Jakob
University of Wuerzburg
294 PUBLICATIONS **8,419** CITATIONS
SEE PROFILE

Robert Edelman
NorthShore University HealthSystem
423 PUBLICATIONS **21,703** CITATIONS
SEE PROFILE

Magnetic Resonance in Medicine 41:1009–1022 (1999)

Signal-to-Noise Ratio and Signal-to-Noise Efficiency in SMASH Imaging

Daniel K. Sodickson,[1]* Mark A. Griswold,[2] Peter M. Jakob,[2] Robert R. Edelman,[2] and Warren J. Manning[1,2]

A general theory of signal-to-noise ratio (SNR) in simultaneous acquisition of spatial harmonics (SMASH) imaging is presented, and the predictions of the theory are verified in imaging experiments and in numerical simulations. In a SMASH image, multiple lines of *k*-space are generated simultaneously through combinations of magnetic resonance signals in a radiofrequency coil array. Here, effects of noise correlations between array elements as well as new correlations introduced by the SMASH reconstruction procedure are assessed. SNR and SNR efficiency in SMASH images are compared with results using traditional array combination strategies. Under optimized conditions, SMASH achieves the same average SNR efficiency as ideal pixel-by-pixel array combinations, while allowing imaging to proceed at otherwise unattainable speeds. The *k*-space nature of SMASH reconstructions can lead to oscillatory spatial variations in noise standard deviation, which can produce local enhancements of SNR in particular regions. Magn Reson Med 41:1009–1022, 1999. © **1999 Wiley-Liss, Inc.**

Key words: SNR; SMASH imaging; fast imaging; RF coil arrays

Radiofrequency (RF) coil arrays are commonly used to improve signal-to-noise ratio (SNR) in magnetic resonance images. However, spatial information from RF coil arrays may also be used to accelerate MR image acquisition by shifting some of the burden of spatial encoding away from the traditional imaging gradients. Since the initial development of MR coil arrays, a number of rapid imaging techniques have been proposed based on this principle (1–9). Recently, using the simultaneous acquisition of spatial harmonics (SMASH) technique (9), two- to fourfold improvements in imaging speed have been demonstrated in vivo with commercial arrays, and up to eightfold accelerations have been obtained in phantom images using specialized RF hardware (10,11). SMASH operates by substituting linear combinations of component coil signals for time-consuming phase-encoding gradient steps, effectively allowing the acquisition of multiple lines of *k*-space in parallel. This approach may be used to multiply the intrinsic speed of MR imaging sequences without increasing gradient switching rate or RF power deposition.

While the SNR properties of various reconstruction algorithms in traditional gradient-encoded acquisitions with coil arrays have been studied in detail (12,13), no similarly detailed studies have documented the effects on image SNR of accelerated parallel data acquisition in arrays. Carlson and Minemura (8) predicted an approximate $\sqrt{2}$ decrease in SNR for a twofold increase in imaging speed using two nested volume coils, and they also predicted spatial variations in SNR across the image plane, but no explicit SNR measurements were reported. In the proposal by Ra and Rim (5) for an alternative image-domain ''subencoding'' approach using surface coils, SNR was not discussed. Kwiat et al (6,7) presented general SNR considerations for a proposed many-coil massively parallel imaging apparatus. These general considerations, however, do not indicate what SNR is to be expected for a partially parallel imaging technique such as SMASH.

In this report, a detailed description of SNR in SMASH imaging is presented. Analytic expressions for the propagation of signal and noise terms in a SMASH reconstruction are derived. These expressions are used to explore the effects of noise correlations on image SNR, the dependence of SNR upon reconstruction parameters, and the scaling of SNR with acquisition speed. SNR and SNR efficiency in SMASH are also compared with theoretical predictions for conventional gradient-encoded acquisitions and image reconstructions using RF coil arrays (12,13).

These theoretical results are then verified in phantom imaging experiments and in numerical simulations. For realistic coil array designs, SMASH images and reference images are compared to assess the spatial distribution and acquisition-speed dependence of SNR. Noise variance measurements for in vivo images are also compared both with theoretical predictions and with the results of simulations.

Finally, after a review of the principal determinants of SNR in SMASH images, implications for the design and use of RF coil arrays in ultrafast partially parallel imaging applications are discussed.

THEORY

SMASH Imaging: A Summary

The SMASH procedure is summarized in Fig. 1. The left-hand side of the figure shows *k*-space schematics for the various stages of data collection and reconstruction, and the right-hand side shows Fourier-transformed image data from a water phantom at each of the corresponding stages.

First, MR signal data are acquired simultaneously in the component coils of an RF coil array. A fraction $1/M$ of the usual number of phase encoding gradient steps are ap-

[1]Charles A. Dana Research Institute and Harvard-Thorndike Laboratory of the Department of Medicine, Cardiovascular Division, Beth Israel Deaconess Medical Center, Boston, Massachusetts.

[2]Department of Radiology, Beth Israel Deaconess Medical Center, Boston, Massachusetts.

Grant sponsor: Whitaker Foundation (Biomedical Engineering Grant).

*Correspondence to: Daniel K. Sodickson, Cardiovascular Division, Beth Israel Deaconess Medical Center, 330 Brookline Avenue, Boston, MA 02215. E-mail: dsodicks@caregroup.harvard.edu

Received 13 February 1998; revised 10 December 1998; accepted 11 December 1998.

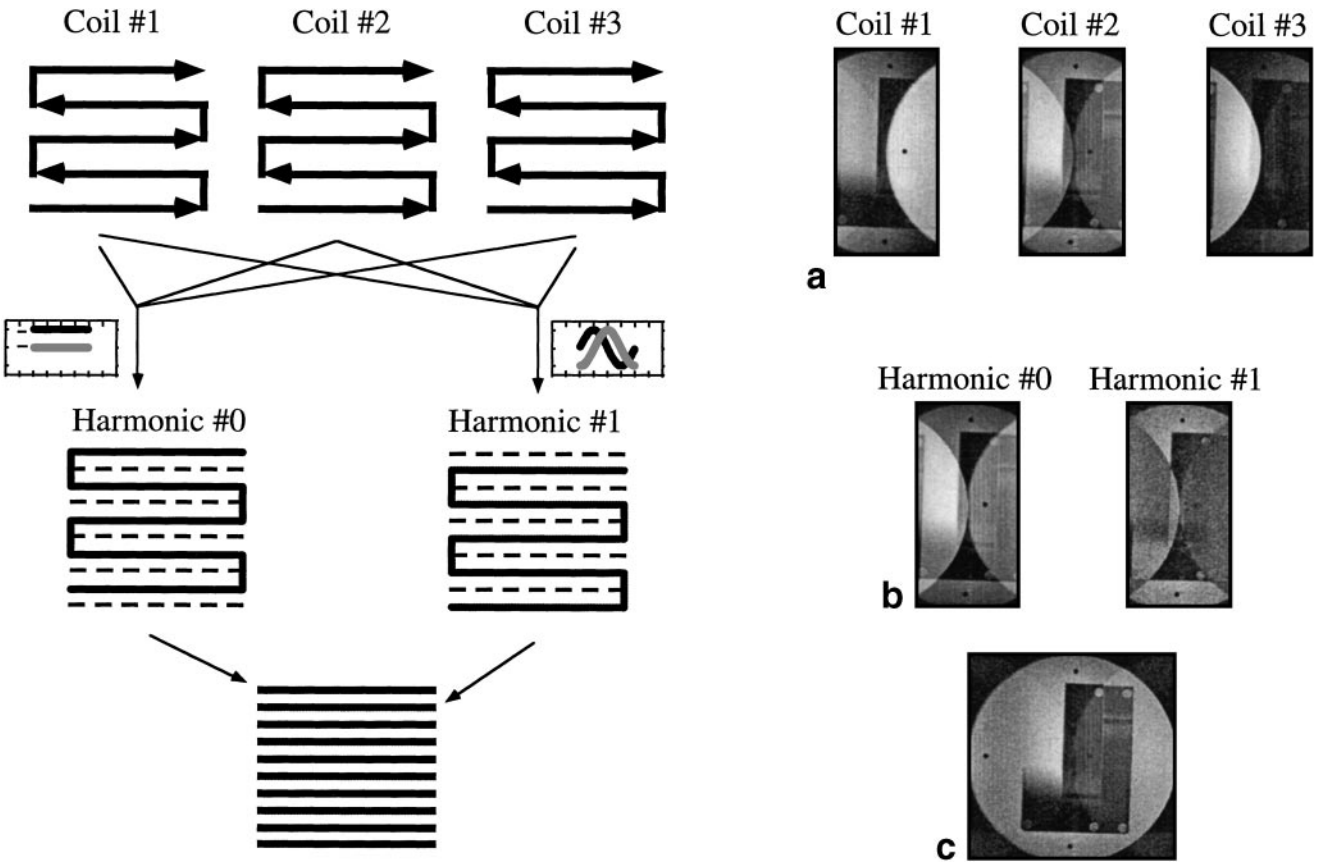

FIG. 1. Schematic representation of the SMASH imaging procedure (*k*-space cartoon on the left, corresponding phantom images on the right). **a:** Simultaneous acquisition of data with a reduced number of phase-encoding gradient steps in multiple component coils of an array. **b:** Formation of shifted data sets using spatial harmonic combinations of component coil signals. **c:** Interleaving of shifted data sets to generate a full signal matrix, corresponding to an image with full FOV in a reduced total acquisition time.

plied, with M times the usual spacing in k-space ($M = 2$ for this schematic example). The component coil signals acquired in this way correspond to images with a fraction $1/M$ of the desired field of view (FOV) (Fig. 1a). With M times fewer phase-encoding steps, only a fraction $1/M$ of the time usually required for this FOV is spent on data collection.

Next, a total of M linear combinations of the component coil signals are formed, to produce M shifted composite signal data sets (Fig. 1b). The linear combinations are designed to produce sinusoidal modulations of total RF sensitivity across the image plane. These modulations, or ''spatial harmonics,'' mimic the modulations produced by phase-encoding gradients and may be shown to produce an identical k-space shift (cf. Ref. 9 and Eq. [4] below). Two such spatial harmonic modulations are illustrated schematically in Fig. 1, for a total time savings factor of $M = 2$ in this example. The maximum achievable time savings factor depends on the total number of spatial harmonics that may reliably be synthesized through linear combination, and this number in turn scales up with the number of array elements. Identification of the appropriate linear combinations for spatial harmonic generation requires independent measurement or estimation of the sensitivity profiles of each component coil in the array. Several strategies for sensitivity calibration have been described (9,14,15). Following calibration, optimal weighting factors for the component coils may be derived from a simple numerical optimization procedure.

After linear combinations have yielded the shifted data sets, these composite signals are interleaved to yield a full k-space matrix appropriate to the full desired FOV. Finally, this matrix is Fourier transformed to give the reconstructed image (Fig. 1c). Since the need for multiple phase-encoding gradient steps generally constitutes the temporal bottleneck in MR acquisitions, the SMASH procedure reduces image acquisition times by an amount proportional to the number of phase-encoding gradient steps omitted, namely, by an integer factor of M. Further details about practical implementations may be found in Ref. 9.

The success of a SMASH reconstruction relies upon the existence of correlations between signals in different component coils of an RF coil array. These signal correlations arise from spatial variations in coil sensitivity. The signal from each array element may be written as

$$S_l(k_x, k_y) = \int\int dx\, dy\, \rho(x, y) C_l(x, y) \exp(-ik_x x - ik_y y) \quad [1]$$

where $\rho(x, y)$ represents the spin density in a two-dimensional image plane labeled by Cartesian coordinates x and y, and $C_l(x, y)$ represents the spatial distribution of RF sensitivity for the l^{th} component coil in the array. k_x and

k_y are k-space coordinates corresponding to evolution in frequency-encoding (G_x) and phase-encoding (G_y) gradients, respectively. Here, a two-dimensional imaging experiment has been assumed, and this assumption will be maintained for the purposes of notational simplicity in the sections that follow. The generalization to three-dimensional imaging is straightforward, however, and three-dimensional imaging sequences have been successfully combined with SMASH in practice.

SMASH relies on the fact that, for a suitable array, the component coil sensitivity functions may be combined with complex weights $\{n_l^{(m)}\}$ to approximate various spatial harmonic profiles of order m. The $m = 0$ harmonic represents the composite sensitivity formed by some reference linear combination with weights $\{n_l^{(0)}\}$, i.e.,

$$C^{(0)}(x, y) = \sum_l n_l^{(0)} C_l(x, y). \quad [2]$$

For the simple case of a linear coil array with elements disposed, for example, along the y direction, it is straightforward to show that higher order harmonics may also be approximated by appropriate weighted sums:

$$C^{(m)}(x, y) = \sum_l n_l^{(m)} C_l(x, y) \approx C^{(0)}(x, y) \exp(-imk_y y). \quad [3]$$

Here, $\Delta k_y = 2\pi/FOV$, and m is an integer that may be positive or negative depending on the direction of k-space shift that is desired. Using Eqs. [1] to [3], we may derive a simple expression for weighted combinations of component coil signals:

$$\begin{aligned}\sum_l n_l^{(m)} S_l(k_x, k_y) &= \iint dx\, dy\, \rho(x, y) \sum_l n_l^{(m)} C_l(x, y) \\ &\quad \cdot \exp(-ik_x x - ik_y y) \\ &\approx \iint dx\, dy\, \rho(x, y) C^{(0)}(x, y) \\ &\quad \cdot \exp(-ik_x x - i(k_y + m\Delta k_y) y) \\ &\approx \iint dx\, dy\, \rho(x, y) \sum_l n_l^{(0)} C_l(x, y) \\ &\quad \cdot \exp(-ik_x x - i(k_y + m\Delta k_y) y) \\ &\approx \sum_l n_l^{(0)} S_l(k_x, k_y + m\Delta k_y) \quad [4]\end{aligned}$$

This is the basic relation underlying SMASH imaging. It illustrates that linear combinations of component coil signals may in fact be used to produce k-space shifts analogous to those produced by magnetic field gradients. It also indicates that, when imaging is performed in a suitably configured RF coil array, the set of MR signal data at one k-space position is linearly related to the signal data at adjacent k-space positions. This is a departure from the usual state of affairs for single-coil imaging, in which such interdependencies between different k-space signals are precluded by the orthogonality of the Fourier basis. An accurate description of SNR in SMASH must also account for any noise correlations that may accompany these k-space signal correlations.

SNR in SMASH: Signal Correlations and Noise Correlations

In this section, we explore the effects of noise correlations, including both preexisting correlations resulting from the sample and array geometry and new correlations introduced by the reconstruction procedure. We have previously reported (9) that when the weights $\{n_l^{(m)}\}$ used for linear combination of component coil signals form orthogonal sets for different spatial harmonics m, no new noise correlations are introduced by the SMASH reconstruction, even though a reduced number of measured data points are being used to generate the final composite image. To lend mathematical rigor to these general arguments, and to study the impact of component coil weighting on SNR, we assess how signal and noise terms propagate through the various stages of the SMASH reconstruction procedure. In the derivation to follow, we will use a discrete index rather than a continuous variable to specify the k-space signal. In other words, the notation $S(k_x, k_y)$ from Eqs. [1] to [4] above will be replaced by the simpler expression S_k.

The image intensity I_j at any pixel j in an MR image may be written as a linear combination of N measured signal points S_k:

$$I_j = \frac{1}{N} \sum_{k=0}^{N-1} W_{jk} S_k. \quad [5]$$

For standard phase warp imaging, W_{jk} is an appropriate coefficient from the inverse Fourier transform, i.e.,

$$W_{jk} = \exp\left(\frac{2\pi ijk}{N}\right). \quad [6]$$

To avoid undue complexity in the equations, only one pixel index j has been used here, and the linear combination in Eq. [5] describes a one-dimensional inverse discrete Fourier transform (DFT). The generalization to multiple dimensions is straightforward, since the non-array-encoded direction has the standard behavior and may be treated with a separate inverse DFT.

When a coil array is used for image acquisition, multiple signal points S_{kl} are acquired simultaneously in each measurement step, one data point for each component coil l. These component coil signals transform into multiple component coil images I_{jl}, where l varies from 1 to L, with L representing the total number of array elements.

In a SMASH image reconstruction, linear combinations of component coil signals are used to generate composite signals that are shifted in k-space. Suppose that, as is illustrated in Fig. 1, all but a fraction $1/M$ of the required k-space positions have been omitted from the acquisition, to yield component coil images with $1/M$ of the desired

FOV. In this case, the k-space index will take values of $k = 0, M, 2M, \ldots, N$, and a total of M linear combinations will be required to fill in the missing data at k-space positions $k + m$, where $m = 1,2, \ldots, M - 1$:

$$S^{\mathrm{SMASH}}_{k+m} = \sum_{l=1}^{L} n_l^{(m)} S_{kl}. \quad [7]$$

To obtain the SMASH-reconstructed full-FOV image, we take the inverse DFT of the composite signal set (including the unshifted $m = 0$ composite), i.e.,

$$I_j^{\mathrm{SMASH}} = \frac{1}{N} \sum_k \sum_{m=0}^{M-1} W_{j,k+m} S^{\mathrm{SMASH}}_{k+m}$$

$$= \frac{1}{N} \sum_k \sum_{m=0}^{M-1} \sum_{l=1}^{L} W_{j,k+m} n_l^{(m)} S_{kl}. \quad [8]$$

The SNR of the SMASH-reconstructed image pixel in Eq. [8] may be expressed in terms of its real and imaginary parts,

$$SNR(\mathrm{Re} I_j^{\mathrm{SMASH}}) = \frac{\langle \mathrm{Re} I_j^{\mathrm{SMASH}} \rangle}{\sigma_{\mathrm{Re} I_j^{\mathrm{SMASH}}}}$$

$$SNR(\mathrm{Im} I_j^{\mathrm{SMASH}}) = \frac{\langle \mathrm{Im} I_j^{\mathrm{SMASH}} \rangle}{\sigma_{\mathrm{Im} I_j^{\mathrm{SMASH}}}} \quad [9]$$

where the brackets indicate a mean value and σ represents the standard deviation over an ensemble of images sampled from the same noise distribution. The numerators in this expression are simply the mean of the real or imaginary parts of Eq. [8], namely,

$$\left\langle \begin{Bmatrix} \mathrm{Re} \\ \mathrm{Im} \end{Bmatrix} I_j^{\mathrm{SMASH}} \right\rangle = \frac{1}{N} \sum_k \sum_m \sum_l \left\langle \begin{Bmatrix} \mathrm{Re} \\ \mathrm{Im} \end{Bmatrix} (W_{j,k+m} n_l^{(m)} S_{kl}) \right\rangle. \quad [10]$$

The denominators in Eq. [9] take a somewhat more complicated form. They may be calculated by taking the variance of real or imaginary components of Eq. [8],

$$\sigma^2_{[\mathrm{Re\ Im}] I_j^{\mathrm{SMASH}}} = \left\langle \left(\begin{Bmatrix} \mathrm{Re} \\ \mathrm{Im} \end{Bmatrix} I_j^{\mathrm{SMASH}} \right)^2 \right\rangle - \left\langle \begin{Bmatrix} \mathrm{Re} \\ \mathrm{Im} \end{Bmatrix} I_j^{\mathrm{SMASH}} \right\rangle^2 \quad [11]$$

and collecting all nonvanishing cross-terms between different component coils l and spatial harmonics m. These cross-terms are evaluated assuming that the distribution of noise in the measured signal points S_{kl} is Gaussian, with zero mean and variance σ^2. Noise voltages for different k-space sample points are assumed independent, since noise is not spatially encoded and is independent of position in the image. Correlation of noise voltages between different array elements is expressed in the usual way by a symmetric noise correlation matrix $\mathbf{R}$ whose elements $R_{ll'}$ express the net noise coupling between component coils l and l', whether from residual mutual inductance not eliminated by array design, or from shared flux of transient current paths in a conductive sample (cf. Refs. 12 and 13). The relevant cross-terms may be expressed as follows:

$$\langle \mathrm{Re} S_{kl} \mathrm{Re} S_{k'l'} \rangle - \langle \mathrm{Re} S_{kl} \rangle \langle \mathrm{Re} S_{k'l'} \rangle$$

$$= \langle \mathrm{Im} S_{kl} \mathrm{Im} S_{k'l'} \rangle - \langle \mathrm{Im} S_{kl} \rangle \langle \mathrm{Im} S_{k'l'} \rangle = \delta_{kk'} R_{ll'} \sigma^2 \quad [12]$$

$$\langle \mathrm{Re} S_{kl} \mathrm{Im} S_{k'l'} \rangle - \langle \mathrm{Re} S_{kl} \rangle \langle \mathrm{Im} S_{k'l'} \rangle$$

$$= \langle \mathrm{Im} S_{kl} \mathrm{Re} S_{k'l'} \rangle - \langle \mathrm{Im} S_{kl} \rangle \langle \mathrm{Re} S_{k'l'} \rangle = 0. \quad [13]$$

Substitution of Eqs. [12] and [13] into an expanded expression for Eq. [11] yields the following result for noise variance in a SMASH reconstruction:

$$\sigma^2_{\mathrm{Re} I_j^{\mathrm{SMASH}}} = \sigma^2_{\mathrm{Im} I_j^{\mathrm{SMASH}}} = \frac{\sigma^2}{N} \frac{1}{M} \sum_m \sum_{m'} \cdot \mathrm{Re} \left(W_{j,m-m'} \sum_l \sum_{l'} n_l^{(m)} R_{ll'} n_{l'}^{*(m')} \right). \quad [14]$$

The sums over l and l' in Eq. [14] express the effects of preexisting noise correlations between array elements prior to SMASH reconstruction, as described by the elements $R_{ll'}$ of the noise resistance matrix. The sums over m and m', on the other hand, describe new noise correlations arising from the reconstruction procedure, as a consequence of the fact that different linear combinations of the *same* acquired data sets have been used to generate *different* lines of k-space.

Combining Eq. [14] with Eqs. [10] and [9] gives the SNR for a SMASH reconstruction:

$$SNR(I_j^{\mathrm{SMASH}}) = \frac{\sum_k \sum_m \sum_l \langle W_{j,k+m} n_l^{(m)} S_{kl} \rangle}{N^{1/2} \sigma \left(\frac{1}{M} \sum_m \sum_{m'} \mathrm{Re} \left(W_{j,m-m'} \sum_l \sum_{l'} n_l^{(m)} R_{ll'} n_{l'}^{*(m')} \right) \right)^{1/2}}. \quad [15]$$

SNR in Fully Gradient-Encoded Acquisitions

Simple Linear Combinations

For reference, suppose that a full data set S^{full}_{kl} is acquired in the same coil array using the same underlying imaging sequence as in the SMASH acquisition. Now k takes its full set of N values, $k = 0, 1, 2, \ldots, N - 1$. Since M times as many phase-encoding gradient steps are now required, the total acquisition time will be M times as long as for the SMASH image. In the interest of making as direct a comparison as possible, we first use a simple linear combination of component coil signals to form the composite reference image I_j^{simple}:

$$I_j^{\mathrm{simple}} = \frac{1}{N} \sum_{k=0}^{N-1} W_{jk} S_k^{\mathrm{full}} = \frac{1}{N} \sum_{k=0}^{N-1} \sum_{l=1}^{L} W_{jk} n_l^{(0)} S^{\mathrm{full}}_{kl}. \quad [16]$$

Here, $n_l^{(0)}$ are the same weights as were used for the $m = 0$ combination in the SMASH reconstruction. A simplified derivation analogous to the one outlined in the previous section yields the following expressions for noise variance and SNR:

$$\sigma^2_{\mathrm{Re}I_j^{\mathrm{simple}}} = \sigma^2_{\mathrm{Im}I_j^{\mathrm{simple}}} = \frac{\sigma^2}{N}\sum_l \sum_{l'} n_l^{(0)} R_{ll'} n_{l'}^{*(0)} \qquad [17]$$

and

$$SNR(I_j^{\mathrm{simple}}) = \frac{\sum_k \sum_l \langle W_{jk} n_l^{(0)} S_{kl}^{\mathrm{full}} \rangle}{N^{1/2}\sigma \left(\sum_l \sum_{l'} n_l^{(0)} R_{ll'} n_{l'}^{*(0)} \right)^{1/2}}. \qquad [18]$$

Optimal Pixel-by-Pixel Phased Array Image Combinations

The simple reference combination, while a convenient benchmark for SMASH SNR, does not represent the best available image combination algorithm from the point of view of SNR. Roemer et al (12) showed that the optimal SNR for a coil array may be achieved on a pixel-by-pixel basis by using appropriate linear combinations of corresponding pixels in each of the component coils. In particular, Roemer et al derived optimal sets of weights $\{n_{jl}\}$ for pixel-by-pixel combinations of the form

$$I_j^{\text{pixel-by-pixel}} = \sum_{l=1}^{L} n_{jl} I_{jl}^{\mathrm{full}} = \frac{1}{N}\sum_l n_{jl} \sum_k W_{jk} S_{kl}^{\mathrm{full}}. \qquad [19]$$

For such a combination, the general expression for SNR is

$$SNR(I_j^{\text{pixel-by-pixel}}) = \frac{\left\langle \sum_l n_{jl} \sum_k W_{jk} S_{kl}^{\mathrm{full}} \right\rangle}{N^{1/2}\sigma \left(\sum_l \sum_{l'} n_{jl} R_{ll'} n_{jl'}^{*} \right)^{1/2}}. \qquad [20]$$

The best solution for complex data combination was shown to involve the noise resistance matrix and the complex conjugate of the coil sensitivity functions:

$$n_{jl}^{\mathrm{optimal}} = \lambda_j \sum_{l'} (R)^{-1}_{ll'} C^*_{jl'}. \qquad [21]$$

Here, λ_j is a free scaling factor that can vary with each pixel without affecting SNR. Ref. 12 also explores a variety of alternative weighting options that may be used in place of the optimal weights of Eq. [21]. The sum of squares combination procedure, which is now widely used for image combination in the absence of detailed sensitivity information, is not, strictly speaking, a linear technique in the sense of Eq. [19]. For linear array designs of the sort described in Ref. 12, however, it has been shown to approximate an optimal linear weighting based on RF sensitivities.

Comparison of SNR in SMASH Versus Fully Gradient-Encoded Acquisitions

Comparison With Simple Linear Combinations: Orthonormality Conditions

How does SMASH SNR (Eq. [15]) compare with the SNR of the simple linear combination (Eq. [18])? Let us consider what happens when the following condition is met:

$$\sum_l \sum_{l'} n_l^{(m)} R_{ll'} n_{l'}^{*(m')} = \delta_{m,m'} \sum_l \sum_{l'} n_l^{(m)} R_{ll'} n_{l'}^{*(m)} \qquad [22]$$

Subject to this constraint, the m' sum in Eq. [14] vanishes, and, using $W_{j0} = 1$, the noise variance becomes

$$\sigma^2_{\mathrm{Re}I_j^{\mathrm{SMASH}}} = \sigma^2_{\mathrm{Im}I_j^{\mathrm{SMASH}}} = \frac{\sigma^2}{N}\frac{1}{M}\sum_m \sum_l \sum_{l'} n_l^{(m)} R_{ll'} n_{l'}^{*(m)}. \qquad [23]$$

(Due to the symmetry of $R_{ll'}$, the sum $\Sigma_l \Sigma_{l'}\ n_l^{(m)} R_{ll'} n_{l'}^{*(m)}$ is purely real, and the Re operator may be omitted.) This expression has a familiar form, similar to that derived in Refs. 12 or 13 for the noise variance of traditional array combinations. The final noise variance in either case is just a square-weighted sum of the variances σ^2 of individual signal points, with mixing dictated by the off-diagonal elements of the noise resistance matrix. The effects of preexisting noise correlations remain in the $R_{ll'}$ term, but no additional noise correlations are introduced by the reconstruction procedure. Comparison of Eq. [23] with Eq. [17] shows that the noise variances $\sigma^2_{\mathrm{Re}I_j^{\mathrm{SMASH}}}$ and $\sigma^2_{\mathrm{Re}I_j^{\mathrm{simple}}}$ are identical whenever

$$\frac{1}{M}\sum_m \sum_l \sum_{l'} n_l^{(m)} R_{ll'} n_{l'}^{*(m)} = \sum_l \sum_{l'} n_l^{(0)} R_{ll'} n_{l'}^{*(0)}. \qquad [24]$$

Ideally, the numerator of the SNR will be the same for the simple reference and the SMASH images, since for a perfect SMASH reconstruction, the composite k-space matrix is identical to the reference matrix of the simple linear combination:

$$S_{k+m}^{\mathrm{SMASH}} = \sum_l n_l^{(m)} S_{kl} = \sum_l n_l^{(0)} S_{k+m,l}^{\mathrm{full}} = S_{k+m}^{\mathrm{simple}}. \qquad [25]$$

In other words, the sum over k and m in the SMASH case reduces identically to a sum over the full range of k in the simple reference image, and

$$\langle I_j^{\mathrm{simple}} \rangle = \left\langle \frac{1}{N}\sum_{k=0}^{N-1} \sum_{l=1}^{L} W_{jk} n_l^{(0)} S_{kl}^{\mathrm{full}} \right\rangle$$

$$= \left\langle \frac{1}{N}\sum_k \sum_{m=0}^{M-1} \sum_{l=1}^{L} W_{j,k+m} n_l^{(m)} S_{kl} \right\rangle = \langle I_j^{\mathrm{SMASH}} \rangle. \qquad [26]$$

Thus, if the SMASH weights allow for an accurate reconstruction and obey both Eqs. [22] and [24], then both signal and noise terms will be equivalent to their counterparts in the simple reference image, and $SNR(I_j^{\mathrm{SMASH}}) =$

$SNR(I_j^{\text{simple}})$, despite the reduced acquisition time of the SMASH image.

What is the meaning of the conditions in Eqs. [22] and [24]? For simplicity, we use a vector notation, expressing the weights $\{n_l^{(m)}\}$ as elements of L-component complex vectors $\mathbf{n}^{(m)}$. The noise resistance matrix $\mathbf{R}$ is a symmetric $L \times L$ matrix that operates on these vectors. In this notation, Eq. [15] becomes

$$SNR(I_j^{\text{SMASH}}) = \frac{\sum_k \sum_m \langle W_{j,k+m} \mathbf{n}^{(m)\dagger} \cdot \mathbf{S}_k \rangle}{N^{1/2} \sigma \left(\frac{1}{M} \sum_m \sum_{m'} \text{Re}\,(W_{j,m-m'} \mathbf{n}^{(m')\dagger} \cdot \mathbf{R} \mathbf{n}^{(m)}) \right)^{1/2}} \quad [27]$$

(where the † symbol denotes the Hermitian conjugate, or the conjugate transpose). Similarly, Eqs. [22] and [24] become

$$\mathbf{n}^{(m)\dagger} \cdot \mathbf{R} \mathbf{n}^{(m')} = \delta_{m,m'} \mathbf{n}^{(m)\dagger} \cdot \mathbf{R} \mathbf{n}^{(m)} \quad [28]$$

$$\frac{1}{M} \sum_m \mathbf{n}^{(m)\dagger} \cdot \mathbf{R} \mathbf{n}^{(m)} = \mathbf{n}^{(0)\dagger} \cdot \mathbf{R} \mathbf{n}^{(0)}. \quad [29]$$

We may define new effective weight vectors $\tilde{\mathbf{n}}^{(m)}$ using the following transformation:

$$\tilde{\mathbf{n}}^{(m)} \equiv (\mathbf{R}^{1/2}) \mathbf{n}^{(m)} \quad [30]$$

which also yields the conjugate relation

$$\tilde{\mathbf{n}}^{(m)\dagger} \equiv \mathbf{n}^{(m)\dagger} (\mathbf{R}^{1/2})^\dagger = \mathbf{n}^{(m)\dagger} (\mathbf{R}^{1/2}). \quad [31]$$

(Here we have used the fact that since $\mathbf{R}$ is symmetric, $\mathbf{R}^{1/2}$ is also symmetric, i.e., $\mathbf{R}^{1/2} = (\mathbf{R}^{1/2})^\dagger$).

In this new basis, $\mathbf{n}^{(m)\dagger} \cdot \mathbf{R} \mathbf{n}^{(m')} \rightarrow \tilde{\mathbf{n}}^{(m)\dagger} \cdot \tilde{\mathbf{n}}^{(m')}$, and Eq. [28] takes a simple form:

$$\tilde{\mathbf{n}}^{(m)\dagger} \cdot \tilde{\mathbf{n}}^{(m')} = \delta_{m,m'} |\tilde{\mathbf{n}}^{(m)}|^2. \quad [32]$$

This is an orthogonality relation for the weights used to generate different harmonics m and m'. Equation [23] describes the noise variance of the SMASH-reconstructed image for the idealized case in which an orthogonal set of effective weights has been used for the reconstruction and embodies the principle with which we began our investigations, namely, that orthogonal linear combinations introduce no new noise correlations.

Similarly, in the new basis, Eq. [29] becomes

$$\frac{1}{M} \sum_m |\tilde{\mathbf{n}}^{(m)}|^2 = |\tilde{\mathbf{n}}^{(0)}|^2. \quad [33]$$

This constitutes a normalization condition for the weight sets $\{\tilde{\mathbf{n}}^{(m)}\}$. For the noise variance of the SMASH image to be equal to the variance of the simple reference image, the various SMASH weight sets must on average have the same norm as $\tilde{\mathbf{n}}^{(0)}$.

In summary, a SMASH image, obtained in a fraction $1/M$ of the total acquisition time, will have the same SNR as a comparable full-time reference image formed by simple linear combination, subject to the orthogonality and normalization conditions

$$\sum_l \sum_{l'} n_l^{(m)} R_{ll'} n_{l'}^{*(m')} = \delta_{m,m'} \sum_l \sum_{l'} n_l^{(m)} R_{ll'} n_{l'}^{*(m)} \text{ (orthogonality)} \quad [34]$$

$$\frac{1}{M} \sum_m \sum_l \sum_{l'} n_l^{(m)} R_{ll'} n_{l'}^{*(m)} = \sum_l \sum_{l'} n_l^{(0)} R_{ll'} n_{l'}^{*(0)} \text{ (normalization).} \quad [35]$$

Whether the SMASH weights approach orthonormality in practice depends on the constraints of spatial harmonic fitting for any particular image plane and coil array geometry. Sample weights are given in a section on experimental results to follow. The simplifying conditions of orthonormality are by no means a requirement for useful SMASH imaging, but they do serve as a design goal for practical array design, and as a helpful conceptual tool for understanding and predicting SNR behavior. For example, departures from orthonormality will have a number of predictable consequences for SNR.

Orthogonality: By virtue of the presence of DFT coefficients $W_{j,m-m'}$, the expression Eq. [14] for noise variance contains both constant terms (with $m = m'$) and oscillating terms (with $m \neq m'$). The oscillatory terms, which, like $W_{j,m-m'}$, have zero mean, characterize spatial *variations* in the value of noise variance across the image. These spatial variations are the result of noise correlations between different k-space lines in the reconstructed signal matrix and are present whenever the orthogonality condition Eq. [34] is violated. In such cases, the operation of the DFT on the partially correlated signal data can lead not only to noise correlations, but also to noise *anticorrelations* in certain areas of the image, resulting in local *reductions* of noise variance. In the $M = 2$ case, all adjacent k-space lines are similarly correlated, resulting in a sinusoidal first-harmonic oscillation of noise variance about its mean value. At higher values of the acceleration factor M, contributions from higher harmonics enter into the noise variance profile, with the relative magnitude of each contribution determined by the degree to which the corresponding effective weights depart from orthogonality. Thus, orthogonality of the weights controls the spatial distribution of noise in a SMASH image.

Normalization: The value of the constant terms with $m = m'$ in Eq. [14] is determined by the norm of the corresponding effective weights. Thus, normalization of the weights controls the baseline about which noise oscillations occur. If weights for higher harmonics have larger norms than the reference zeroth-harmonic weights, i.e., if $1/M \, \Sigma_m |\tilde{\mathbf{n}}^{(m)}|^2 >$

$|\tilde{\mathbf{n}}^{(0)}|^2$, then baseline SNR will decrease due to an increase in noise variance out of proportion to signal amplitude. On the other hand, if weights for higher harmonics have smaller norm than the reference weights $\tilde{\mathbf{n}}^{(0)}$, average SNR will actually be improved in the SMASH image compared with the reference image formed by simple linear combination.

Comparison With Optimal Pixel-by-Pixel Combinations

The comparison of SMASH SNR with the SNR of optimal pixel-by-pixel combinations is somewhat less straightforward, since the magnitude of SNR gains from pixel-by-pixel techniques depends on the particular structure of component coil sensitivities, which in turn depends on array geometry and image plane orientation. In general, no single closed form comparison exists independent of a particular geometry. Nevertheless, the principal effects of pixel-by-pixel weighting may be estimated using approximate models. The optimal pixel-by-pixel weights have been shown to be proportional to the complex conjugate of the coil sensitivity functions, C_{jl}^{*} (cf. Ref. 12 and Eq. [21]). Such a weighting maintains a maximum additive signal in regions of significant signal amplitude, while discarding, to the greatest extent possible, regions dominated by noise. In other words, the optimal pixel-by-pixel weighting constitutes a form of matched filtering. For linear coil arrays, this pixel-by-pixel noise-filtering effect tends to give SNR gains on the order of $\sqrt{L}$ compared with simple sums of component coil images (where L once again represents the number of array elements). These arguments indicate that, for the linear arrays used in this work, optimal pixel-by-pixel techniques will yield a factor of approximately $\sqrt{L}$ better SNR than SMASH reconstructions with well-normalized weights. Departures from the normalization condition will affect the comparison by shifting the SMASH noise baseline up or down, as was outlined in the previous section. The spatial distribution of SNR in the pixel-by-pixel reconstructions will be determined by the structure of the coil sensitivity functions, whereas in SMASH images the spatial distribution will also be affected by the orthogonality of the weights. The results of detailed SNR comparisons for particular array designs will be presented in sections to follow.

Comparison of SNR Efficiency in SMASH Versus Fully Gradient-Encoded Acquisitions

One particularly noteworthy feature of the expression for SMASH SNR (Eq. [15]) is that, when the orthonormality conditions are met, SNR is independent of the acceleration factor M. In this situation, whether the image is acquired at 2 times or at 10 times the standard sequential imaging speed, the SNR of the SMASH-reconstructed image is the same. A comparison of how SNR scales with acquisition time in partially parallel as opposed to fully gradient-encoded sequential acquisitions is therefore in order.

In traditional sequential imaging, SNR is proportional to the square root of the acquisition time and thus decreases with the square root of imaging speed. This proportionality has been shown to arise from the integration over acquisition time that effectively takes place during Fourier transformation of the MR signal in the course of image generation (16). Inherent in the proportionality, however, is an assumption that total acquisition time scales linearly with matrix size N for any given imaging sequence, since in sequential MRI, each additional line of data requires an additional gradient-encoding step. This assumption no longer holds true in a partially parallel acquisition such as SMASH, for which distinct lines of data are sampled simultaneously, rather than one after the other. To the extent that the various gradient-encoded and coil-encoded lines remain independent of one another, SNR is proportional to the total number of data lines, by virtue of the DFT operation. The conditions for independence of gradient-encoded and coil-encoded lines are just the orthonormality conditions Eqs. [34] and [35]. Thus, for a fixed final matrix size, SNR in a SMASH reconstruction with orthonormal weights is independent of the total encoding time. Departures from orthogonality change the spatial distribution of SNR but do not affect its mean value across the image, which does not decrease with increasing imaging speed unless the normalization of the weights is degraded. By contrast, for purely sequential techniques, an M-fold increase in acquisition speed that preserved matrix size and resolution would either be impossible or else, if possible, would generally be accompanied by a factor of $\sqrt{M}$ reduction in SNR.

Figure 2a contains an idealized plot of expected SNR as a function of acquisition speed for SMASH reconstructions of reduced data sets compared with simple linear combinations or optimal pixel-by-pixel combinations of full data sets in the same coil array. The array in this example is comprised of four component coils with a linear geometry, and the SNR of pixel-by-pixel combinations is assumed to be dominated by the noise-filtering effect. Under these conditions, optimal pixel-by-pixel combinations will have twice the SNR of simple linear combinations. SNR for both of these reference combinations falls in proportion to the square root of acquisition speed. The SMASH reconstructions, on the other hand, begin at the lower SNR of the simple combination, but maintain this value as acquisition speed is increased by integer factors, as long as orthogonality and normalization conditions continue to be met. (Once again, for any set of well-normalized weights, the mean SNR across the image is preserved as acquisition speed increases, regardless of whether or not the weights are orthogonal.) At the maximum achievable acceleration factor, the SMASH curve intersects the curve for an ideal matched filter combination.

Figure 2b shows the same results expressed in terms of SNR efficiency, defined here as SNR per square root acquisition time. Once again, the SMASH curve crosses from the lower baseline of the simple combination to meet the matched filter combination at the maximum acceleration factor. This means that, in the same time as would normally be required for a full acquisition, one could acquire multiple SMASH images, average them together, and obtain the same net SNR as would have been obtained

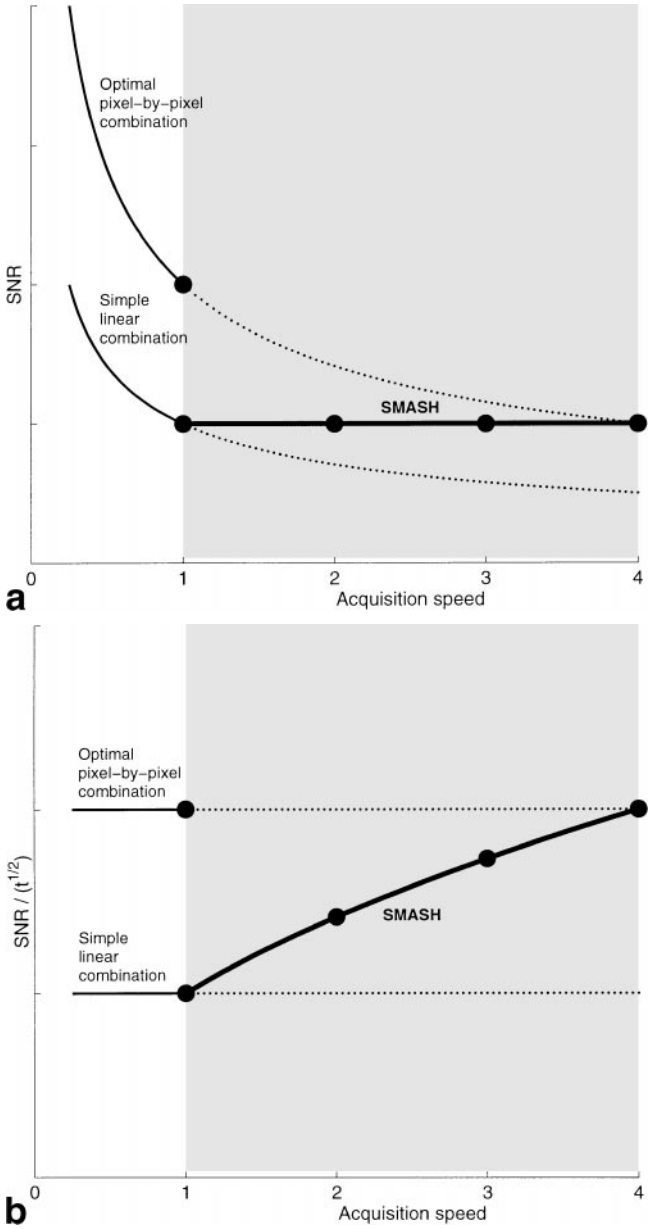

FIG. 2. Idealized plots of expected SNR (**a**) and SNR efficiency (i.e., SNR per unit square root acquisition time; **b**) as a function of acquisition speed for SMASH reconstructions of reduced data sets compared with simple linear combinations or optimal pixel-by-pixel combinations of full data sets. The same four-element array is assumed in all cases, and orthonormal weights are assumed for the SMASH reconstructions. The acquisition speed indicated in the figure as 1 unit is assumed to be the maximum speed that may safely be achieved using sequential imaging techniques, so that speeds in the grayed region are attainable only with partially parallel acquisitions.

for an optimal matched filtered image generated from the full data set.

One of the most promising applications of SMASH, and of parallel imaging in general, will be to allow increases in speed even when physical and physiologic constraints would otherwise prevent further gains. If unit acquisition speed in Fig. 2 is taken to lie at the sequential speed limit (as given by peak gradient performance or by the neuromuscular stimulation threshold, for example), then the gray-shaded areas in the figure represent a range of speeds that may only be achieved using a partially parallel acquisition strategy. The dotted continuations of the simple sum or the pixel-by-pixel SNR curves then represent theoretically predicted but practically unattainable behavior. An optimal SMASH reconstruction has the same SNR as the optimal pixel-by-pixel reconstruction would have *if* the latter could be operated at higher speed.

METHODS

Phantom Imaging Experiments

To verify theoretical predictions, and to explore the behavior of SNR under realistic imaging conditions, a resolution phantom was imaged using a custom-built four-element linear array on a Siemens Vision 1.5 T whole-body clinical MR imager (Siemens Medical Systems, Erlangen, Germany). The array, which consisted of four 78 × 230 mm rectangular elements overlapped along their short axis for a total array extent of 260 × 230 mm, was initially developed for accelerated SMASH imaging of the heart and of the brain (17). For the current studies, the array was oriented in a coronal plane, with the elements disposed along the foot-head B_0 field direction. The image plane was also coronal, and located approximately 40 mm from the array, with a foot-head phase-encoding direction. A fast low-angle shot (FLASH) imaging sequence was used, with TR of 12 msec, TE 6 msec, matrix size 128 × 128, FOV 300 × 300 mm, flip angle 7°, and slice thickness 4 mm. The flip angle and slice thickness were chosen for a target mean reference SNR in the range of 30–40. In this SNR range, the effects of system instabilities (on the order of 1% variation from acquisition to acquisition for our commercial imaging system) lie below the noise level and do not significantly complicate SNR measurements.

After the phantom had been left in place to stabilize for 15 min, 56 separate acquisitions were performed, of which the last 48 were used as a measurement ensemble. (The first eight acquisitions were discarded to avoid any non-steady-state effects such as mechanical vibrations in the fluid compartments of the phantom.) Identical reconstructions for reference and for SMASH images were then performed on each of the 48 data sets. Reference image reconstructions were applied to the full acquired data sets, using either a simple sum of component coil signals or a traditional sum of squares combination algorithm (in which component coil images are combined pixel-by-pixel as the square root of the sum of square magnitudes). SMASH reconstructions were performed on reduced data sets, representing accelerated acquisitions with reduced phase encoding. The weights $\{n_l^{(m)}\}$ for spatial harmonic generation were calculated with a matrix least squares algorithm, using representative signal profiles along the phantom diameter as internal sensitivity references (cf. Ref. 9). Unit weights ($n_l^{(0)} = 1$) were used both for the simple linear combination reference and for the zeroth spatial harmonic

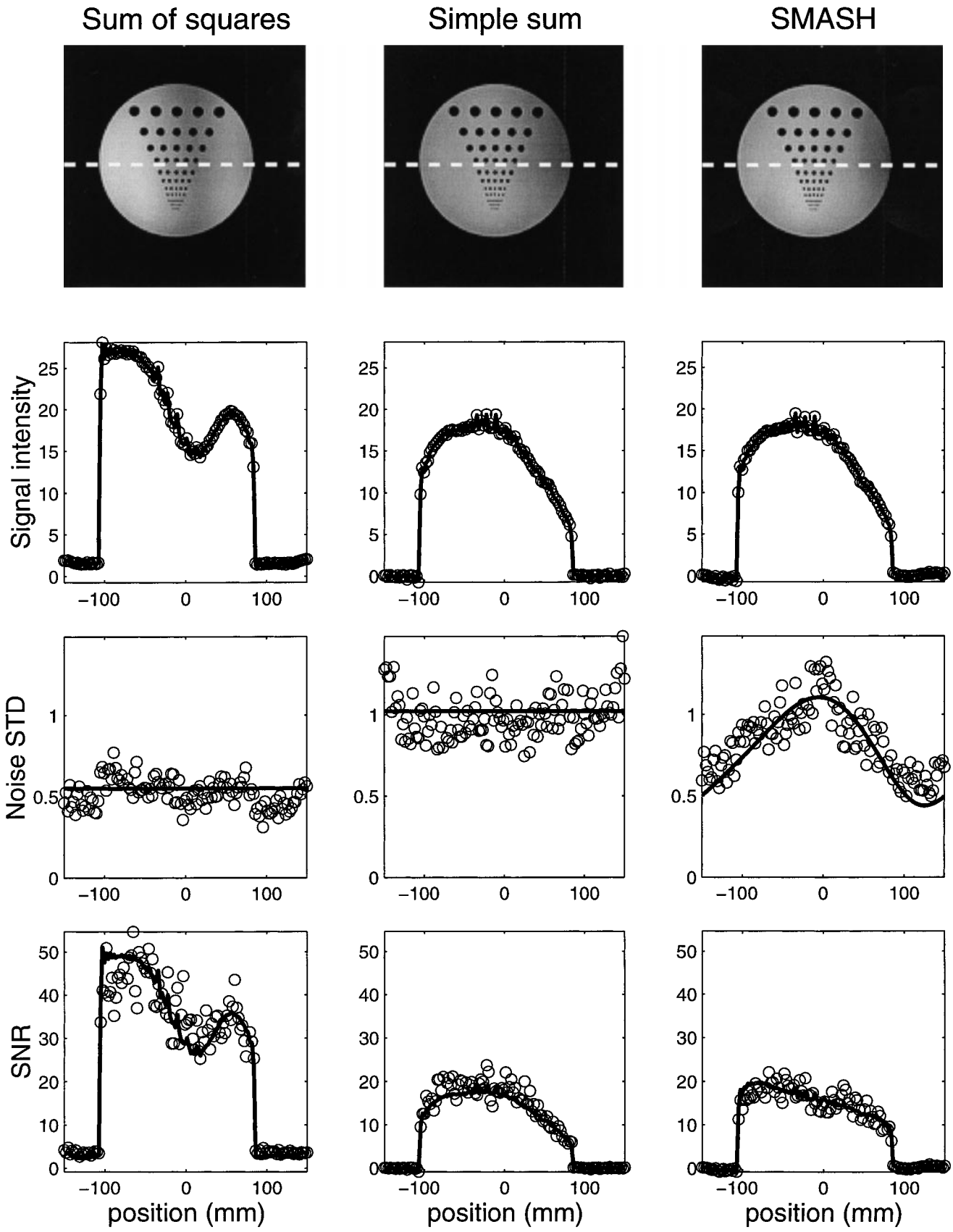

FIG. 3. Spatial distribution of signal intensity, noise standard deviation, and SNR for reference and double-speed SMASH images of a resolution phantom using the four-element array. Open circles, experimental data; solid lines, theoretical predictions. Signal, noise, and SNR profiles were taken along dashed lines in the reconstructed images shown at the top. Image acquisition and reconstruction parameters are reported in the text.

in SMASH reconstructions. (Such a choice, as opposed to a combination that produces homogeneous signal intensity, for example, is allowed in SMASH reconstructions so long as all higher harmonics are multiplied by the ''zeroth harmonic'' profile; cf. Eqs. [2] and [3]).

SNR values were then calculated on a pixel-by-pixel basis by taking the mean of each pixel intensity over the ensemble of reconstructed images and dividing by the standard deviation over the same ensemble. Measured SNR values were compared with theoretical predictions based on the observed signal distributions, the calculated SMASH weights, and the measured noise correlation matrix.

In Vivo Measurements

A combination of numerical simulations and empirical measurements was used to assess the spatial variation of noise in an in vivo imaging situation. MR signal data, image data, and reconstruction parameters from a previous study (9) were used for this analysis. The MR signal data were obtained in a healthy adult volunteer, using the commercial Siemens CP spine array with four active elements on our Siemens Vision 1.5 T system. A centric-reordered single-shot RARE sequence was used, and the FOV was chosen to cover the abdomen and thorax of the volunteer. Further details on imaging parameters are available in Ref. 9. The original image data included a) a reference image acquired in 540 msec and reconstructed using a sum of squares algorithm; and b) a SMASH image acquired in 270 msec with half the number of phase-encoding gradient steps and reconstructed using the SMASH procedure with $M = 2$.

For the simulations, 16 correlated noise sets were added to the original in vivo MR signal data sets, to simulate an ensemble of repeated experimental measurements. Noise was generated by calls to a Gaussian random number generator (the function *randn* in Matlab Version 5.0 (The Mathworks, Natick, MA)), with values of the variance selected to match empirically estimated SNRs in the source images. Correlation of noise between component coils was simulated by multiplying component coil noise sets by a noise correlation matrix R derived from experimental measurements in the appropriately loaded array. After the correlated noise replicas had been added to the source signal sets, an ensemble of reconstructed images was generated using the sum of squares or the SMASH reconstruction algorithms. Pixel-by-pixel calculations of noise standard deviation in this ensemble were compared with theoretical predictions based on the SMASH weights (the same weights used in the original imaging study) and on the measured noise correlation matrix.

For comparison with both theory and simulations, noise standard deviation as a function of position was also measured directly in the original reference and SMASH images. A small rectangular region of interest (ROI) was initially placed in the corner of the in vivo images, and the standard deviation of image intensities within this region was calculated for various ROI positions along the edge of the images in the phase encoding direction. Since each calculation was performed in an ostensibly signal-free region, each constituted an approximate measure of noise standard deviation in that region, and the set of these measurements taken together constituted an estimate of the spatially dependent noise profile.

RESULTS

Phantom Imaging Experiments

Figures 3 and 4 compare experimental results (open circles) with theoretical predictions (solid lines) for SNR as a function of position in phantom images using the four-element array.

Figure 3 plots pixel-by-pixel signal intensity, noise standard deviation, and SNR profiles for sum of squares, simple sum, and SMASH images. Profiles were taken along a diameter of the phantom indicated by dashed lines in the images shown at the top. In signal profile, the double-speed SMASH image is a faithful replica of the full-time simple sum reference profile. Noise profiles are essentially flat for the two reference reconstruction techniques, while the standard deviation profile shows a marked oscillation for the SMASH reconstruction. This oscillation, which closely matches the predicted profile, results from nonorthogonalities of the effective weights used for SMASH reconstruction. Close inspection of the figure shows that the oscillation in noise background corresponds to a relative enhancement of SNR at the edges of the SMASH SNR profile compared with the simple sum SNR profile.

Figure 4 plots noise standard deviation profiles as a function of SMASH acceleration factor M from $M = 2$ to $M = 4$. The effects of higher harmonic contributions to the oscillatory noise profile are particularly evident at $M = 4$. In the SMASH images shown at the right of Fig. 4, slight residual aliasing artifacts may be seen at the higher SMASH factors, as has been described in more detail in Ref. 9. The noise profiles, however, are unaffected by these residual artifacts.

Figure 5 shows the scaling of SNR with imaging speed for phantom images with the four-element array. Mean SNR values were calculated from the reference and SMASH data sets by averaging the pixel-by-pixel SNR over the circular region spanned by the phantom. Mean SNR for the sum of squares combination was 33.3, and is represented in the figure as an open triangle. The simple sum combination (open square) had a mean SNR of 14.8, approximately a factor of 2 lower than for the sum of squares. As in the schematic graph of Fig. 2, dotted lines have been drawn to indicate the theoretically predicted but practically unattainable square-root scaling of these SNR values for higher sequential acquisition speeds. Mean SNR measurements for SMASH reconstructions with acceleration factors of 2 to 4 are represented as open diamonds, connected by a solid line to guide the eye. The measured SMASH SNR values were 14.4 ($M = 2$), 14.5 ($M = 3$), and 13.8 ($M = 4$). (In all cases, estimated measurement error is smaller than the marker size.) The dashed line represents the scaling of SNR with acquisition speed that would be expected for purely orthonormal SMASH weights. The slight depression of measured SNR at $M = 4$ results from a relative

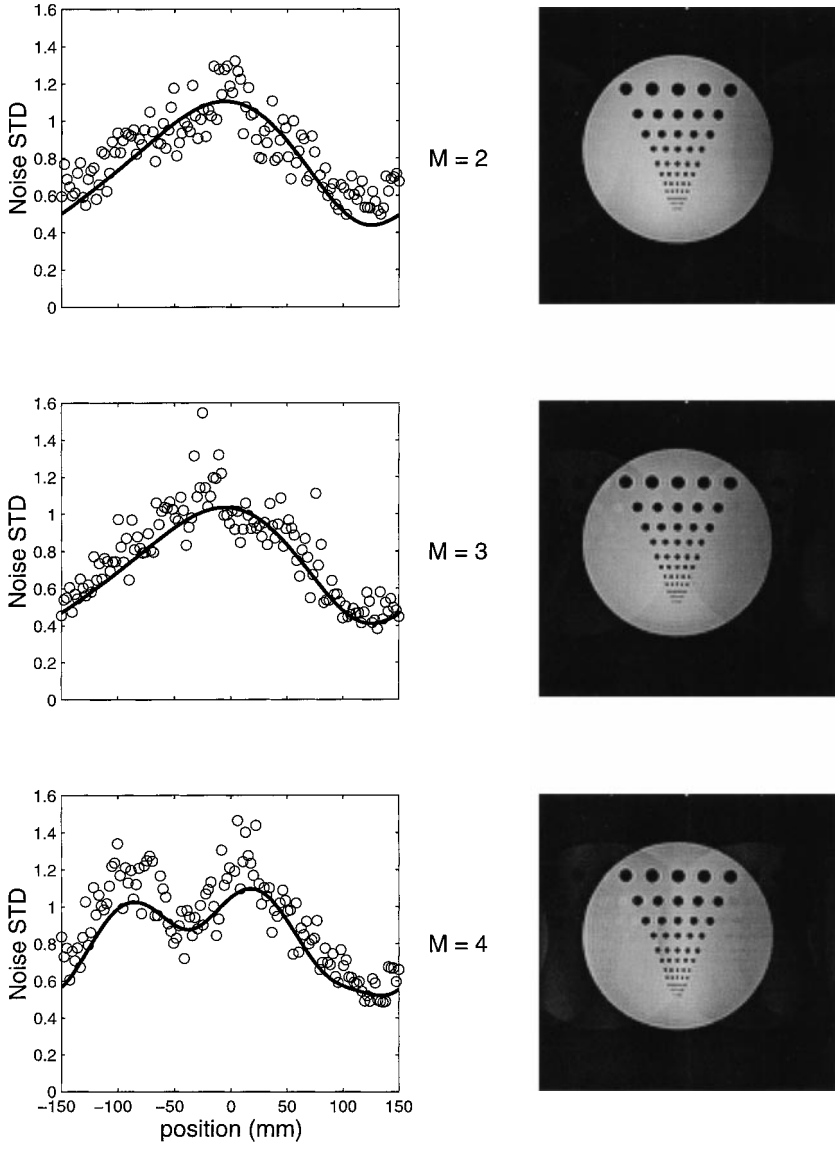

FIG. 4. Noise standard deviation profiles as a function of SMASH acceleration factor *M* for phantom images using the four-element array. Left-hand column, noise profiles, with open circles representing experimental data and solid lines representing theoretical predictions; right-hand column, SMASH-reconstructed images.

increase in the norm of the weights for the highest spatial harmonic used in the reconstruction.

Indeed, all the general features of the SNR profiles in Figs. 3–5 may be predicted from the values of the weights used for image reconstruction. For the phantom experiments described here, these weights were as follows,

	$l=1$	$l=2$	$l=3$	$l=4$
$m=-1$	$0.3+0.7i$	$1.0-0.1i$	$0.2-1.0i$	$-0.6-0.4i$
$m=0$	1	1	1	1
$m=1$	$0.3-0.7i$	$1.0+0.1i$	$0.2+1.0i$	$-0.6+0.4i$
$m=2$	$-0.6-0.7i$	$1.1+0.1i$	$-1.1+0.3i$	$0.4-0.8i$

[36]

where harmonic number runs from $m = -1$ to $m = 2$ down each column, and component coil number runs from $l = 1$ to $l = 4$ along each row. The norms and relative vector angles of these weights may be calculated from dot products of each row in Eq. [36] against itself and against the other rows:

Norm:

$m=-1$	$m=0$	$m=1$	$m=2$
3.2	4.0	3.2	4.2

Angle:

	$m=-1$	$m=0$	$m=1$	$m=2$
$m=-1$	0	71	82	89
$m=0$	71	0	71	74
$m=1$	82	71	0	70
$m=2$	89	74	70	0

[37]

Departures from 90° in the angle matrix of Eq. [37] represent the nonorthogonalities that result in noise variance oscillations in Figs. 3 and 4. Inspection of the weight vector normalizations confirms that the normalization condition of Eq. [35] is met or exceeded for all but the highest harmonic, since only the $m = 2$ harmonic (norm = 4.2) has a larger norm than the $m = 0$ harmonic (norm = 4.0).

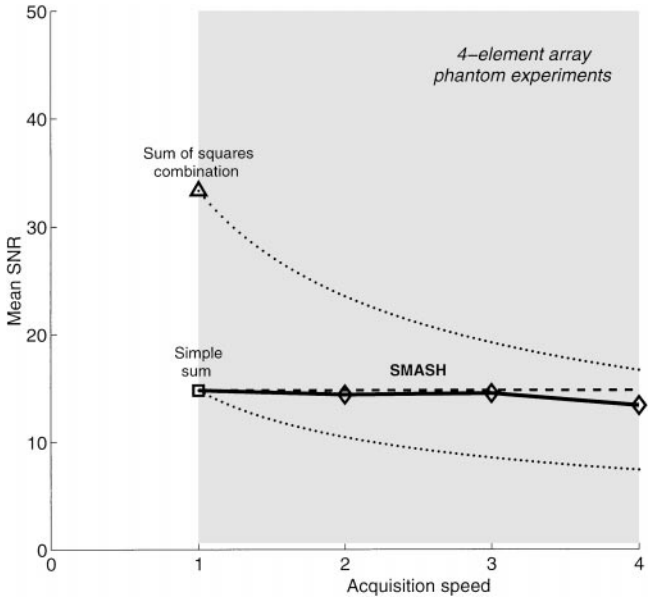

FIG. 5. Mean pixel-by-pixel SNR as a function of acquisition speed for reference and SMASH images of a resolution phantom using the four-element array. Mean SNR was calculated by averaging pixel-by-pixel SNR values in each reference or SMASH image over the circular region spanned by the phantom. Open triangles, sum of squares reference; open squares, simple sum reference; open diamonds connected by solid line, SMASH; dashed line, SNR that would be expected for orthonormal effective SMASH weights. SMASH acceleration factors range from $M = 2$ to $M = 4$. As in Fig. 2, dotted lines represent reference SNR values that would be expected if equivalent speed increases were possible using sequential techniques alone.

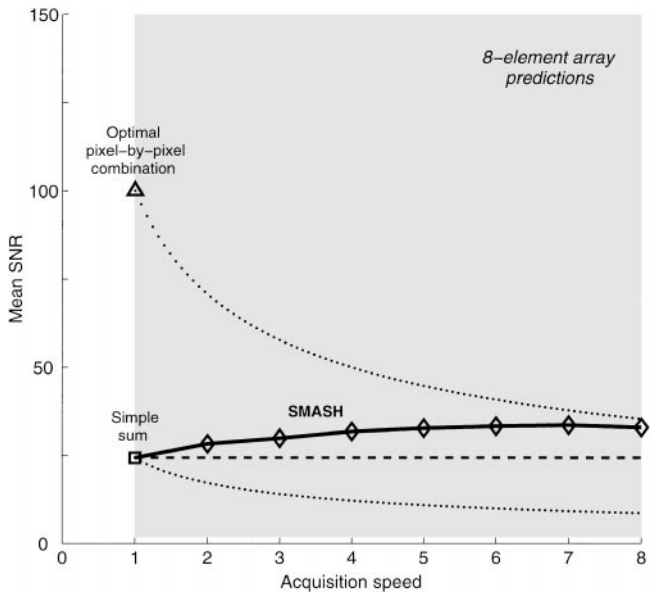

FIG. 6. Mean pixel-by-pixel SNR as a function of acquisition speed for sample SMASH image reconstructions in an eight-element array, as predicted from properties of the weights in Eq. [38]. Open triangles, sum of squares reference; open squares, simple sum reference; open diamonds connected by solid line, SMASH; dashed line, SNR that would be expected for orthonormal effective SMASH weights. SMASH acceleration factors range from $M = 2$ to $M = 8$. As in Fig. 2, dotted lines represent reference SNR values that would be expected if equivalent speed increases were possible using sequential techniques alone.

We emphasize that the theoretical curves in Figs. 3–5 are exact results calculated from Eq. [15], making no appeal to orthonormality. The principles of orthogonality and normalization serve, however, as useful tools for predicting SNR behavior using only a small set of component coil weights as a priori information. For example, the norms and overlap angles for a sample SMASH reconstruction in the eight-element array used elsewhere to achieve eightfold accelerations (10,11) are as follows:

Norm:

$m = -3$	$m = -2$	$m = -1$	$m = 0$	$m = 1$	$m = 2$	$m = 3$	$m = 4$
5.9	4.5	5.7	12.7	5.7	4.5	5.8	7.8

Angle:

	$m = -3$	$m = -2$	$m = -1$	$m = 0$	$m = 1$	$m = 2$	$m = 3$	$m = 4$
$m = -3$	0	86	81	79	88	86	86	82
$m = -2$	86	0	89	75	82	89	86	89
$m = -1$	81	89	0	78	77	82	88	89
$m = 0$	79	75	78	0	78	75	79	81
$m = 1$	88	82	77	78	0	90	82	83
$m = 2$	86	89	82	75	90	0	86	77
$m = 3$	86	86	88	79	82	86	0	77
$m = 4$	82	89	89	81	83	77	77	0

[38]

Figure 6 shows the mean SNR as a function of acceleration factor predicted from these weights. Though residual nonorthogonalities do remain, a large number of the overlap angles in this case approach 90°, and noise variance oscillations are expected to be significantly smaller than those shown in Fig. 4 (a fact easily confirmed by simulations). Furthermore, the favorable normalization behavior allows a nearly optimal average SNR efficiency at the highest SMASH factors.

In Vivo Measurements

Noise oscillations in an in vivo SMASH image are documented in Fig. 7. For purposes of orientation, reference sum of squares and SMASH images, reproduced from Ref. 9, are included in the top panel, with the shifted positions of the noise measurement region indicated by adjacent boxes with diamonds on the two images. The solid diamonds in the plots beneath show the corresponding mea-

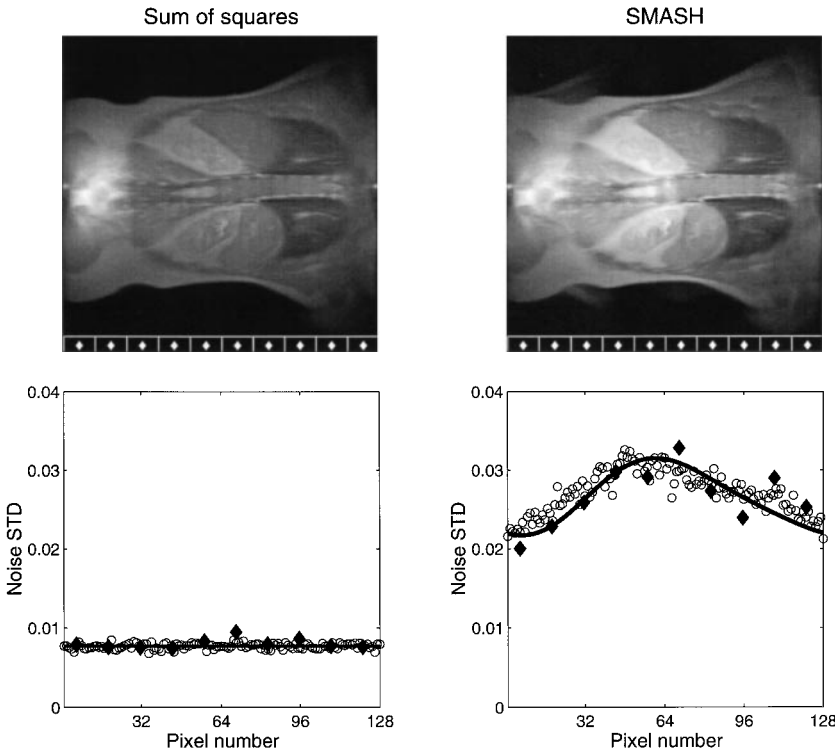

FIG. 7. Noise standard deviation as a function of position in the phase-encoding direction for an in vivo data set (from a scan of the abdomen and thorax of a healthy adult volunteer using a single-shot RARE sequence). Top row, sum of squares reference image (left) and double-speed SMASH image (right). Boxes with diamonds indicate positions of the region of interest for measurements of noise standard deviation. Bottom row, measured, simulated, and theoretically predicted noise standard deviation as a function of position. Solid diamonds, measured noise standard deviation in the boxed regions indicated on the images above; open circles, noise standard deviation profile based on 16 simulated replicas; solid lines, theoretically predicted noise standard deviation profiles.

sured noise standard deviations as a function of box position. Also included in these plots are the simulated standard deviation profile (open circles) and the predictions of the theory (solid lines). As may be seen, the in vivo measurements agree well both with simulations and with theory. Given the substantial spatial variations shown here, it is clear that traditional empirical SNR estimation techniques, which measure signal and noise in different regions of the image, must be approached with caution in SMASH imaging.

DISCUSSION

As has been demonstrated in the theoretical and experimental investigations presented here, SNR in a SMASH imaging study depends in general on the preexisting degree of noise correlation in the coil array used for imaging, and on the weight factors used for SMASH reconstruction. These two determinants may be combined into a single set of effective weights, $\{\tilde{n}_l^{(m)}\}$, as defined in Eq. [30]. Normalization of the effective weights controls the *average* noise level in the SMASH image, and a departure from the normalization condition raises or lowers baseline SNR by altering the noise out of proportion to the signal. On the other hand, orthogonality of the effective weights controls the *spatial distribution* of noise. A departure from orthogonality introduces correlations between adjacent lines of *k*-space, which in turn leads to predictable oscillatory variations in noise standard deviation across the image.

Image plane orientation and coil array geometry are the principal determinants of SMASH weight factors. In practice, the weights can vary significantly as the position and orientation of the image plane with respect to the coil array is varied, with large tilt angles away from the plane of the array generally leading to reductions in SNR as a result of degraded normalization behavior. However, the phantom experiments of Fig. 5 and the predictions of Fig. 6 show that favorable normalization behavior can be achieved at least for image planes parallel to realistic arrays. In the future, tailored array designs may be developed to optimize average SNR for particular anatomical regions or imaging applications.

The presence of noise variance oscillations in SMASH images raises another interesting possibility for coil array design. Since these noise variance oscillations are not necessarily accompanied by oscillations in image intensity, it may be possible to engineer arrays that have localized SNR ''hot spots'' in particular regions of interest. This would involve a deliberate selection for particular *nonorthogonal* weights, such that SNR is maximized in anatomic regions of interest, at the expense of SNR in less interesting outlying regions.

Additional sequence-dependent effects not explicitly considered in this article can also influence SNR in a SMASH image reconstruction. For example, in single-shot sequences such as echoplanar imaging, SNR can be recovered to some extent by virtue of the faster acquisition itself, due to reduced relaxation and hence reduced attenuation of central *k*-space lines in an accelerated echo train. Thus, the final SNR in any given SMASH image may result from a balance of sequence-specific and reconstruction-specific factors.

The SMASH technique operates by exploiting correlations between the MR signals in different array elements. The presence of such correlations suggests that when data are acquired in an array of spatially distinct component coils, a certain redundancy is introduced into the tradi-

tional MR spatial encoding procedure using field gradients. Using appropriate reconstruction strategies, some of the redundant information may be extracted from the data. Such a line of argument naturally leads to the question of whether SMASH, or similar partially parallel imaging schemes, may be used to enhance the total achievable SNR in MR images. If SNR may be preserved in reduced acquisition times, then one would expect that the time saved could then be applied for SNR enhancement, for example, via additional signal averaging. When SMASH images are compared with images from a single RF coil, or with simple combinations of component coil images in RF coil arrays, such an averaging procedure would indeed yield an improved SNR. Optimized SMASH reconstructions represent true increases in SNR per unit time over these reference images. Such references are admittedly nonoptimal, however, since optimal pixel-by-pixel array combinations have been shown to have a higher baseline SNR. While SMASH uses the redundancy inherent in multiple component coil signals to increase imaging speed, the optimal pixel-by-pixel approach abides by the traditional limits on acquisition speed, but resolves the redundancy instead in a way that maximizes SNR for a given acquisition. This dichotomy is inherent in the use of MR coil arrays: the acquisition and reconstruction strategy may be designed to optimize either for SNR or for speed, or else for some intermediate combination of the two. There is no evidence at present suggesting that the pixel-by-pixel optimum derived by Roemer et al (12) may be exceeded on the basis of reconstruction strategy alone. However, sequence-dependent effects alluded to earlier, such as diminished relaxation in accelerated single-shot images, may eventually allow net gains in SNR efficiency using partially parallel acquisitions.

CONCLUSIONS

SMASH may be used to increase MR imaging speed without increasing gradient switching rate or RF power deposition, generally with some absolute penalty in SNR, but with the potential for preserved average SNR efficiency. The theory, simulations, and experimental results presented in this article identify the key parameters that influence SNR in a SMASH acquisition and image reconstruction. An understanding of these parameters may be used to guide coil array design for the optimization of SNR in applications of rapid and ultra-rapid parallel MRI.

ACKNOWLEDGMENTS

The authors have benefited from many lively discussions of the vicissitudes of signal and noise with a number of interested colleagues. D.K.S. acknowledges helpful suggestions from Drs. Peter Roemer, Zhi-Pei Liang, and Randy Duensing.

REFERENCES

1. Carlson JW. An algorithm for NMR imaging reconstruction based on multiple RF receiver coils. J Magn Reson 1987;74:376–380.
2. Hutchinson M, Raff U. Fast MRI data acquisition using multiple detectors. Magn Reson Med 1988;6:87–91.
3. Kelton JR, Magin RL, Wright SM. An algorithm for rapid image acquisition using multiple receiver coils. In: Proceedings of the SMRM Eighth Annual Meeting, 1989. p 1172.
4. Ra JB, Rim CY. Fast imaging method using multiple receiver coils with subencoding data set. In: Proceedings of the SMRM Tenth Annual Meeting, 1991. p 1240.
5. Ra JB, Rim CY. Fast imaging using subencoding data sets from multiple detectors. Magn Reson Med 1993;30:142–145.
6. Kwiat D, Einav S, Navon G. A decoupled coil detector array for fast image acquisition in magnetic resonance imaging. Med Phys 1991;18: 251–265.
7. Kwiat D, Einav S, Navon G. Preliminary experimental evaluation of an inverse source imaging procedure using a decoupled coil detector array in magnetic resonance imaging. Med Eng Phys 1995;17:257–263.
8. Carlson JW, Minemura T. Imaging time reduction through multiple receiver coil data acquisition and image reconstruction. Magn Reson Med 1993;29:681–688.
9. Sodickson DK, Manning WJ. Simultaneous acquisition of spatial harmonics (SMASH): fast imaging with radiofrequency coil arrays. Magn Reson Med 1997;38:591–603.
10. Sodickson DK, Bankson JA, Griswold MA, Wright SM. Eightfold improvements in MR imaging speed using SMASH with a multiplexed eight-element array. In: Proceedings of the ISMRM Sixth Scientific Meeting and Exhibition, 1998. p 577.
11. Bankson JA, Griswold MA, Wright SM, Sodickson DK. An eight-element linear array for SMASH imaging. In: Proceedings of the ISMRM Sixth Scientific Meeting and Exhibition, 1998.
12. Roemer PB, Edelstein WA, Hayes CE, Souza SP, Mueller OM. The NMR phased array. Magn Reson Med 1990;16:192–225.
13. Hayes CE, Roemer PB. Noise correlations in data simultaneously acquired from multiple surface coil arrays. Magn Reson Med 1990;16: 181–191.
14. Jakob PM, Griswold MA, Edelman RR, Sodickson DK. AUTO-SMASH, a self-calibrating technique for SMASH imaging. In: Proceedings of the ISMRM Sixth Scientific Meeting and Exhibition, 1998. p 1975.
15. Jakob PM, Griswold MA, Edelman RR, Sodickson DK. AUTO-SMASH: a self-calibrating technique for SMASH imaging. MAGMA 1998;7: 42–54.
16. Macovski A. Noise in MRI. Magn Reson Med 1996;36:494–497.
17. Griswold MA, Jakob PM, Edelman RR, Sodickson DK. An RF array designed for cardiac SMASH imaging. In: Proceedings of the ISMRM Sixth Scientific Meeting and Exhibition, 1998. p 437.